

Interplay between Energetic and Kinetic Factors on the Ambient Stability of n-Channel Organic Transistors Based on Perylene Diimide Derivatives

Joon Hak Oh,[†] Ya-Sen Sun,[†] Rüdiger Schmidt,[§] Michael F. Toney,[‡] Dennis Nordlund,[‡] Martin Könemann,^{||} Frank Würthner,[§] and Zhenan Bao^{*,†}

[†]Department of Chemical Engineering, Stanford University, 381 North South Mall, Stanford, California 94305, [‡]Stanford Synchrotron Radiation Lightsource, Stanford Linear Accelerator Center, 2575 Sand Hill Road, M/S 69, Menlo Park, California 94025, [§]Universität Würzburg, Institut für Organische Chemie and Röntgen Research Center for Complex Material Systems, Am Hubland, D-97074 Würzburg, Germany, and ^{||}BASF SE, GVP/C, D-67056 Ludwigshafen, Germany

Received August 17, 2009. Revised Manuscript Received October 8, 2009

The effects of the interplay between energetic and kinetic factors on the air stability of n-channel organic thin-film transistors (OTFTs) were studied using two perylene diimide (PDI) compounds with distinctly different lowest unoccupied molecular orbital (LUMO) levels. On the basis of the empirical energy level windows, one compound (*N,N'*-bis(2,2,3,3,4,4,5,5,5-nonafluoropentyl)-3,4:9,10-tetracarboxylic acid diimide (PDI-F): -3.84 eV) is at the onset region for air stability, whereas the other (*N,N'*-bis(cyclohexyl)-1,7-dicyano-perylene-3,4:9,10-tetracarboxylic acid diimide (PDI-CN₂): -4.33 eV) is in the air-stable region. Charge-transport behaviors under an inert atmosphere and in air were investigated as a function of active layer thickness. Charge transport in air was greatly affected by the active layer thickness for both compounds, an effect that has been overlooked so far. The ambient stability of the air-unstable PDI-F TFTs increased significantly for thicknesses over ~ 10 monolayers (ML). Surprisingly, the previously considered “air-stable” PDI-CN₂ TFTs were not stable in air if the active layer thickness was less than ~ 4 ML. The molecular packing and orientation of the PDI thin films were investigated using grazing incidence X-ray diffraction (GIXD) and near-edge X-ray absorption fine structure (NEXAFS). We found that the minimum thickness required for air stability is closely related to the LUMO level, film morphology, and film growth mode.

Introduction

Understanding and controlling charge transport in organic thin-film transistors (OTFTs) has been an active research area during the past decade. This has proven to critically depend on the packing of the organic molecules, degree of order in the solid state, energetic barriers at electrode contacts, as well as on the semiconductor/dielectric interfacial properties.^{1,2} Despite their intrinsic potential as ambipolar semiconductors with both p-type (hole transporting) and n-type (electron transporting) conduction,³ the majority of organic semiconductors practically exhibit unipolar transport, typically p-type transport, because the energetically high-lying LUMO in most organic semiconductors hinders the efficient injection of electrons from the contact to the LUMO.

Moreover, electron charge carriers are vulnerable to trapping by ambient oxidants, such as O₂, H₂O, or O₃.^{3–6} Therefore, one major challenge in OTFT research is to develop high performance n-channel organic semiconductors; these are essential for complementary circuits offering low power consumption, high operating speed, and device stability against operational parameter variations and external noise.^{7,8}

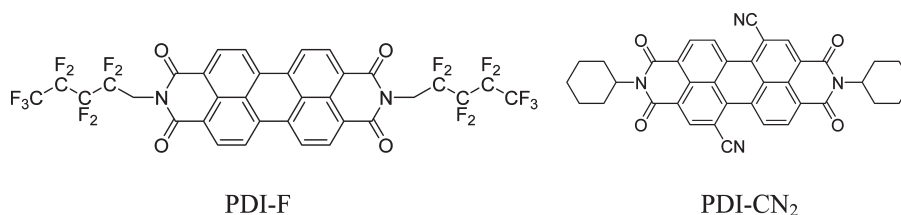
The strategies to stabilize field-induced electron charge carriers in OTFTs can be classified into three categories: (i) semiconductor design to lower the LUMO level, (ii) electrode contact modification, and (iii) interface engineering between the dielectric and semiconductor. The first strategy, based on molecular orbital energetics, is to make π -conjugated cores of organic semiconductors electron-deficient (electron-accepting) by substitution with strong electron-withdrawing and/or hydrophobic

*Corresponding author. E-mail: zbao@stanford.edu.

- (1) Bao, Z.; Locklin, J. *Organic Field-Effect Transistors*; Taylor: Boca Raton, FL, 2007; Vol. 1.
- (2) Coropceanu, V.; Cornil, J.; da Silva Filho, D. A.; Olivier, Y.; Silbey, R.; Bredas, J.-L. *Chem. Rev.* **2007**, *107*, 926–952.
- (3) Chua, L. L.; Zaumseil, J.; Chang, J. F.; Ou, E. C. W.; Ho, P. K. H.; Sirringhaus, H.; Friend, R. H. *Nature* **2005**, *434*, 194–199.
- (4) Weitz, R. T.; Amsharov, K.; Zschieschang, U.; Villas, E. B.; Goswami, D. K.; Burghard, M.; Dosch, H.; Jansen, M.; Kern, K.; Klauk, H. *J. Am. Chem. Soc.* **2008**, *130*, 4637–4645.

- (5) Jones, B. A.; Facchetti, A.; Wasielewski, M. R.; Marks, T. J. *J. Am. Chem. Soc.* **2007**, *129*, 15259–15278.
- (6) Chabiny, M. L.; Street, R. A.; Northrup, J. E. *Appl. Phys. Lett.* **2007**, *90*, 123508.
- (7) Klauk, H.; Zschieschang, U.; Pfau, J.; Halik, M. *Nature* **2007**, *445*, 745–748.
- (8) Crone, B.; Dodabalapur, A.; Lin, Y. Y.; Filas, R. W.; Bao, Z.; LaDuca, A.; Sarpeshkar, R.; Katz, H. E.; Li, W. *Nature* **2000**, *403*, 521–523.

Chart 1. Organic Semiconductors Investigated in This Work



substituents such as F,^{9,10} CN,¹¹ Cl,¹² alkanoyl,¹³ perfluorobenzene,¹⁴ and fluoroalkyl groups.^{15–17} This yields air-stable n-channel operation by significantly lowering the LUMO of the resulting molecule to resist ambient oxidation. The second approach, in terms of charge injection, is to minimize the injection energy barrier from the electrode to the LUMO by employing electrodes with low workfunctions.^{18,19} The third, developed more recently, is to eliminate deep electron trapping sites by passivating the dielectric/semiconductor interface.^{3,12,20,21}

It is well-known that charge transport in OTFTs takes place predominantly in the first few monolayers (MLs) of organic semiconductor near the semiconductor/dielectric interface.^{1,2,22} Systematic studies on ultrathin films of p-channel organic semiconductors revealed that the thickness of the charge transport layer is materials dependent. For example, in transistors made from vacuum-deposited α -hexathienylene (α -6T) films, the induced charges reside in the first two MLs.^{22,23} On the other hand, in vacuum-deposited pentacene TFTs, the field-effect mobility takes about 6 MLs before the maximum current output is reached.²⁴ For the ML structure of pentacene on SiO₂, two pentacene molecules in the unit cell stand vertically on the substrate, unlike the molecules in the thin film phase (long molecular axis tilt angle ~ 5 – 6°).²⁵ The

difference in semiconductor layer thickness needed to reach the maximum current may originate from the differences in film growth mode and film morphology, which are affected by the dielectric surface properties. Although the studies on the thickness dependence of mobility for p-channel OTFTs have been well-documented,^{22–26} few such studies have been carried out for n-channel OTFTs. The thickness dependence of n-channel OTFT performance is of particular interest, because this will permit a better understanding of the factors contributing to air stability as well as the thickness evolution of film growth and morphology of electron transporting organic semiconductors.

In this study, we fabricated n-channel OTFTs with various thicknesses, from two n-channel organic semiconductors with LUMO levels corresponding to two different, empirical first reduction potential (E_{R1}) windows for arylene diimides: one is at the onset region for air stability (-3.8 to -4.0 eV)²⁷ and the other is in the air-stable region (< -4.3 eV).⁵ We found that charge transport in ambient air for both cases is strongly affected by film thickness—an effect that has received little attention thus far in understanding the ambient stability of n-channel OTFTs. We found that the minimum thickness required for air stability of n-channel semiconductors is closely related to the film morphology and film growth mode, in addition to the LUMO level. Transistors based on ultrathin layers of a core-cyanated perylene diimide derivative (PDI-CN₂, Chart 1), previously reported as an air-stable n-channel organic semiconductor because of its relatively low-lying LUMO (-4.33 eV),¹¹ were not stable in air if the active layer thickness was less than about 4 ML, i.e., below ~ 7 nm. Organic semiconductors with a lower LUMO and/or a dense quasi-layer-by-layer growth mode afford air-stable transistors for a thinner film. To the best of our knowledge, our results demonstrate for the first time the effects of the interplay between energetic and kinetic factors on the air stability of n-channel OTFTs.

Experimental Methods

Materials. PDI-F and PDI-CN₂ were synthesized as reported previously,^{11,17} and purified twice by vacuum sublimation in a three-temperature-zone furnace before deposition.

Instrumentation. A Digital Instruments (DI) MMAFM-2 scanning probe microscope was used to perform tapping-mode AFM on the samples with a silicon tip of 300 kHz frequency. DI

- (9) Bao, Z.; Lovinger, A. J.; Brown, J. J. *Am. Chem. Soc.* **1998**, *120*, 207–208.
- (10) Schmidt, R.; Ling, M. M.; Oh, J. H.; Winkler, M.; Könnemann, M.; Bao, Z. N.; Würthner, F. *Adv. Mater.* **2007**, *19*, 3692–3695.
- (11) Jones, B. A.; Ahrens, M. J.; Yoon, M. H.; Facchetti, A.; Marks, T. J.; Wasielewski, M. R. *Angew. Chem., Int. Ed.* **2004**, *43*, 6363–6366.
- (12) Tang, M. L.; Oh, J. H.; Reichardt, A. D.; Bao, Z. *J. Am. Chem. Soc.* **2009**, *131*, 3733–3740.
- (13) Yoon, M. H.; DiBenedetto, S. A.; Facchetti, A.; Marks, T. J. *J. Am. Chem. Soc.* **2005**, *127*, 1348–1349.
- (14) Yoon, M. H.; Facchetti, A.; Stern, C. E.; Marks, T. J. *J. Am. Chem. Soc.* **2006**, *128*, 5792–5801.
- (15) Katz, H. E.; Lovinger, A. J.; Johnson, J.; Kloc, C.; Siegrist, T.; Li, W.; Lin, Y. Y.; Dodabalapur, A. *Nature* **2000**, *404*, 478–481.
- (16) Facchetti, A.; Mushrush, M.; Katz, H. E.; Marks, T. J. *Adv. Mater.* **2003**, *15*, 33–38.
- (17) Schmidt, R.; Oh, J. H.; Sun, Y.-S.; Deppisch, M.; Krause, A.-M.; Radacki, K.; Braunschweig, H.; Könnemann, M.; Erk, P.; Bao, Z.; Würthner, F. *J. Am. Chem. Soc.* **2009**, *131*, 6215–6228.
- (18) Ahles, M.; Schmechel, R.; Seggern, H. v. *Appl. Phys. Lett.* **2004**, *85*, 4499–4501.
- (19) Tang, Q. X.; Li, H. X.; Liu, Y. L.; Hu, W. P. *J. Am. Chem. Soc.* **2006**, *128*, 14634–14639.
- (20) Kumaki, D.; Umeda, T.; Tokito, S. *Appl. Phys. Lett.* **2008**, *92*, 093309.
- (21) Chen, F.-C.; Liao, C.-H. *Appl. Phys. Lett.* **2008**, *93*, 103310.
- (22) Dodabalapur, A.; Torsi, L.; Katz, H. E. *Science* **1995**, *268*, 270–271.
- (23) Dinelli, F.; Murgia, M.; Levy, P.; Cavallini, M.; Biscarini, F.; de Leeuw, D. M. *Phys. Rev. Lett.* **2004**, *92*, 116802.
- (24) Ruiz, R.; Papadimitratos, A.; Mayer, A. C.; Malliaras, G. G. *Adv. Mater.* **2005**, *17*, 1795–1798.
- (25) Mannsfeld, S. C. B.; Virkar, A.; Reese, C.; Toney, M. F.; Bao, Z. *Adv. Mater.* **2009**, in Press.

- (26) Park, B.-N.; Seo, S.; Evans, P. G. *J. Phys. D: Appl. Phys.* **2007**, *40*, 3506–3511.
- (27) Wang, Z.; Kim, C.; Facchetti, A.; Marks, T. J. *J. Am. Chem. Soc.* **2007**, *129*, 13362–13363.

Nanoscope software was used to process the raw AFM images. Cyclic voltammetry were recorded on a CHI411 instrument. UV-vis was recorded with a Varian Cary 6000i UV-vis spectrophotometer. Samples were prepared in ambient conditions with non-air-free cuvettes.

Grazing incidence X-ray diffraction (GIXD) measurements were carried out at the Stanford Synchrotron Radiation Light-source (SSRL) on beamline 11-3 with photon energy of 12.73 keV. The diffraction patterns were recorded using a 2D image plate detector (MAR345) with a pixel size of 150 μm (2300 \times 2300 pixels). The detector was located at a distance of 400.0 mm from the sample center. The dimensions of the GIXD samples were approximately 10 mm \times 15 mm, with the short side aligned parallel with the beam direction. The incidence angle was chosen in the range of 0.09–0.12° to optimize the signal-to-background ratio. The diffraction patterns were distortion-corrected (θ -dependent image distortion introduced by the planar detector surface) before performing the quantitative analysis on the images. A diffraction pattern obtained for a LaB₆ crystal was used as calibration reference. The overall resolution in the GIXD experiments, dominated by the sample size, was about 0.06–0.1 \AA^{-1} .

To obtain molecular tilting information, near-edge X-ray absorption fine structure (NEXAFS) spectra were collected from PDI-CN₂ and PDI-F thin films with various thicknesses. These experiments were performed on beamline 10-1 at SSRL. The incident X-ray beam is elliptically polarized with 80% horizontal and 20% vertical linear polarizations.²⁸ The carbon K-edge spectra were collected in total electron yield (TEY, by means of the sample drain current) mode over the photon energy range from 260 to 440 eV with an energy resolution of about 80 meV. In this work, angular-dependence Carbon-K-edge spectra were collected at five different angles (20, 40, 55, 70, and 90°). A detailed description of the experiment setup can be found in the literature.²⁸

Device Fabrication and Characterization. Bottom-gate top-contact devices were made according to a literature procedure.²⁹ Highly doped n-type (100) Silicon wafers with thermally grown SiO₂ (300 nm, capacitance per unit area (C_i): $1.0 \times 10^{-8} \text{ F cm}^{-2}$) were used as substrates for fabrication of TFTs. The SiO₂/Si wafers were cleaned with a piranha solution (70:30 H₂SO₄:H₂O₂ by vol %) for 30 min, then copiously rinsed with DI water, and dried using a nitrogen gun (99.9% pure). The SiO₂/Si substrates were subsequently treated with UV-ozone plasma (Jetlight UVO-cleaner model 42 100 V) for 20 min. Octadecyltrimethoxysilane (OTS) treatment was done according to a procedure we reported that forms crystalline OTS by spin-coating.³⁰ The SiO₂/Si substrates were spin-coated with a 3 mM solution of OTS in trichloroethylene, then placed in an environment saturated with ammonia vapor for 12 h, followed by sonication cleaning, sequential washing and drying. PDI semiconductors were vacuum-deposited at a rate of 0.2–0.3 \AA s^{-1} under a pressure of ca. 1×10^{-6} Torr to a target thickness as determined in situ by a calibrated quartz crystal microbalance (QCM). During the deposition, the substrates were kept at elevated temperatures (i.e., 90 and 125° for PDI-F and PDI-CN₂, respectively) that yielded the optimal level of performance. The OTS layer was thermally stable in this temperature range

and the crystalline phase was not changed.^{17,30} Gold was thermally evaporated onto the semiconductor layer to form source and drain electrodes with shadow masks with a channel width (W) to length (L) ratio (W/L) of 20 ($W = 1000 \mu\text{m}$, $L = 50 \mu\text{m}$ and $W = 2000 \mu\text{m}$, $L = 100 \mu\text{m}$). The current–voltage (I – V) characteristics of the devices were measured either in air (the relative humidity 30–45%) or in a nitrogen glovebox (oxygen level < 1 ppm) using a Keithley 4200-SCS semiconductor parameter analyzer. Key device parameters, such as field-effect mobility (μ), on-to-off current ratio ($I_{\text{on}}/I_{\text{off}}$), threshold voltage (V_T), were extracted from the drain-source current (I_{DS}) versus gate-source voltage (V_G) characteristics under the assumptions of conventional transistor equations:²

$$I_{\text{DS}} = \frac{W}{2L} \mu C_i (V_G - V_T)^2 \quad (1)$$

The mobility was determined in the saturation regime from the slope of plots of $(I_{\text{DS}})^{1/2}$ versus V_G .

Results

Thin Film Morphology. To investigate the film growth and morphology, we performed AFM analysis on the PDI thin films with various thicknesses. Figure 1 displays tapping-mode AFM images showing the evolution of PDI-F film morphology on OTS-treated SiO₂/Si as a function of the nominal film thickness. The PDI-F nominal film thickness (Θ) in the number of monolayers (ML) was estimated from the ratio of the target film thickness to the height of a layer of the standing molecules determined by the GIXD out-of-plane $d(001)$ -spacing (1 ML \approx 2.18 nm). As the thickness increased from 1.4 to 1.8 ML, the first layer coverage increased and the nuclei for the second layer started to grow. However, the gaps (empty space) between the first layer grains are large, indicating that a percolation path between source and drain electrodes might not have formed yet. At $\Theta = 2.3$ ML, the PDI-F film formed the second layer consisting of coalesced network of domains, and small nuclei (~ 50 nm in long axis) for the third layer started to form. The number of layers was estimated with section analysis of a longer range of AFM scans including the bottom substrate. The thickness of each layer (2.2 ± 0.2 nm) agrees well with the GIXD out-of-plane $d(001)$ -spacing.

As shown by the AFM image obtained at $\Theta = 2.7$ ML, the third layer growth became dominant after the completion of the second layer. At $\Theta = 5.5$ ML, the third layer was completed, and the fourth layer started nucleating. The thicker layer obtained at $\Theta = 9.2$ ML also showed the upper layer growth became dominant after the underlying layer coverage became large. This indicates that the PDI-F film growth takes place in a quasi-layer-by-layer fashion (Frank-van der Merwe mode),^{31,32} although a small portion of the nucleation for the next layer is observed.

The PDI-CN₂ film thickness was also normalized by the height of a layer of the standing molecules determined

- (28) Lüning, J.; Yoon, D. Y.; Stöhr, J. *J. Electron Spectrosc. Relat. Phenom.* **2001**, *121*, 265–279.
 (29) Locklin, J.; Roberts, M. E.; Mannsfeld, S. C. B.; Bao, Z. *J. Macromol. Sci., Part C: Polym. Rev.* **2006**, *46*, 79–101.
 (30) Ito, Y.; Virkar, A. A.; Mannsfeld, S.; Oh, J. H.; Toney, M.; Locklin, J.; Bao, Z. *J. Am. Chem. Soc.* **2009**, *131*, 9396–9404.

- (31) Venables, J. A.; Spiller, G. D. T.; Hanbucken, M. *Rep. Prog. Phys.* **1984**, *47*, 399–459.
 (32) Forrest, S. R.; Burrows, P. E. *Supramol. Sci.* **1997**, *4*, 127–139.

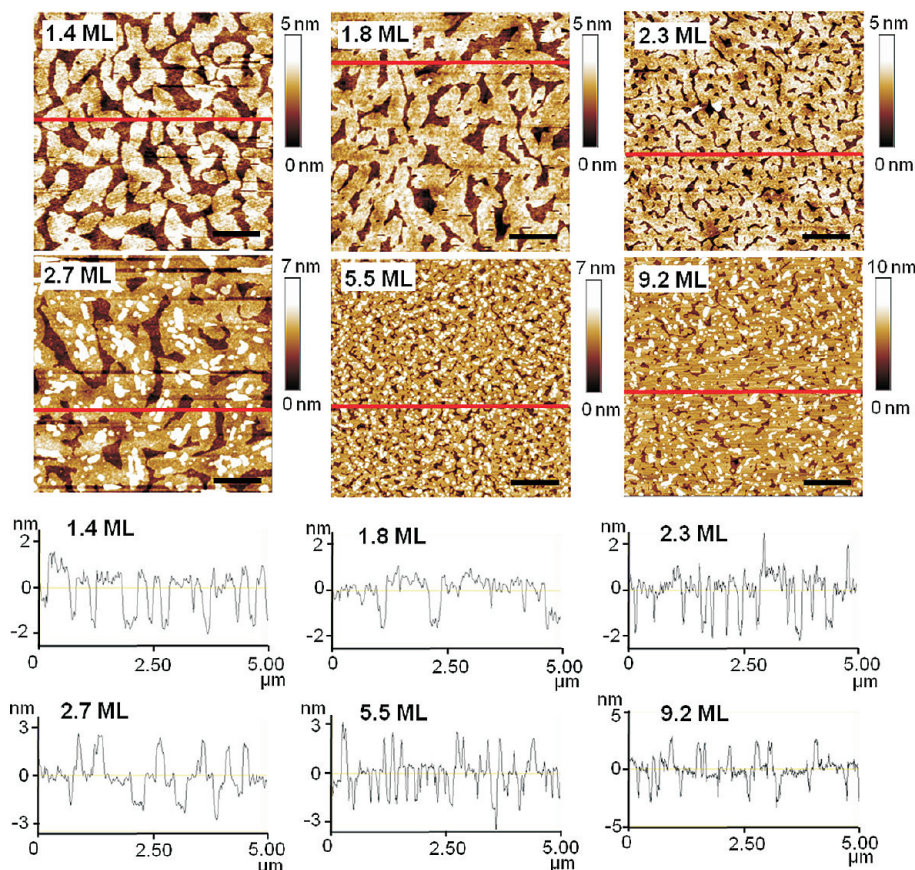


Figure 1. Tapping-mode AFM images of PDI-F thin films for various nominal thicknesses on OTS-treated SiO₂/Si substrate. The scale bar corresponds to 1 μ m.

by the GIXD out-of-plane $d(001)$ -spacing (1 ML \approx 1.84 nm), which is slightly larger than that (1.79 nm) reported in the literature.¹¹ This may be due to the difference in the dielectric surface treatments used. As shown below, we also observed a higher mobility than that reported previously. PDI-CN₂ formed the first coalesced, wetting layer at the initial stage, as shown for $\Theta = 1.6$ ML in Figure 2. However, the subsequent layers nucleated before the completion of the underlying layer, forming more 3D islands. A larger number of islands nucleated in the upper layers for $\Theta > 2$ ML. For example, the nucleation of the fifth layer began at $\Theta = 3.2$ ML, and the seventh at $\Theta = 6.5$ ML. The film growth of PDI-CN₂ follows quasi-Stranski-Krastanov mode,^{31,32} which proceeds by a wetting layer and subsequent islands.

It has been known that different molecular orientations in organic semiconductors, such as vertical or horizontal orientation, or a mixture of both, lead to diverse microstructures in thin films of various thicknesses.³³ To gain more in-depth understanding of the microstructures of the PDI thin films, a combined effort of GIXD and NEXAFS analyses was applied to understand the crystal packing and molecular arrangement in the thin films.

GIXD and NEXAFS Analyses of PDI-F. Figure 3 shows a series of 2D GIXD patterns for PDI-F films of various

thicknesses on OTS-treated surfaces. All the patterns reveal rod-like scattering typical for strongly fiber textured films with cylindrical symmetry: the c -axis of the crystallites of PDI-F molecules is highly oriented with respect to surface normal. For an ultrathin film obtained at $\Theta = 1.4$ ML, we observed several weak Bragg diffraction rods exhibiting the maximum intensity at nonzero q_z (i.e., off the equator); this indicates the formation of a monolayer of PDI-F with molecules that are tilted off the surface normal.³⁴ According to the positions of the Bragg rods, the in-plane reciprocal lattice components were found to be $a^*_{\parallel} = 0.61 \text{ \AA}^{-1}$, $b^*_{\parallel} = 0.82 \text{ \AA}^{-1}$, and $\gamma^*_{\parallel} = 89.5^\circ$, indicative of a nearly rectangular in-plane unit cell. For thicker films, elongated Bragg diffraction spots appeared in the GIXD patterns, typical of the diffraction from thin films of 3D crystals with strong fiber texture.^{35,36} These exhibit higher intensities with increasing film thickness. Based on the positions of the Bragg diffraction peaks, the unit cell for thicker PDI-F films where the films form 3D crystal structures is calculated as a triclinic unit cell with dimensions: $a = 10.3 \text{ \AA}$, $b = 7.8 \text{ \AA}$, $c = 22.2 \text{ \AA}$, $\alpha = 100.4^\circ$, $\beta = 91.6^\circ$, and

(33) DeLongchamp, D. M.; Ling, M. M.; Jung, Y.; Fischer, D. A.; Roberts, M. E.; Lin, E. K.; Bao, Z. *J. Am. Chem. Soc.* **2006**, *128*, 16579–16586.

(34) Als-Nielsen, J.; Jacquemain, D.; Kjaer, K.; Leveiller, F.; Lahav, M.; Leiserowitz, L. *Phys. Rep.* **1994**, *246*, 251–313.

(35) Breiby, D. W.; Bunk, O.; Andreasen, J. W.; Lemke, H. T.; Nielsen, M. M. *J. Appl. Crystallogr.* **2008**, *41*, 262–271.

(36) Yuan, Q.; Mannsfeld, S. C. B.; Tang, M. L.; Roberts, M.; Toney, M. F.; DeLongchamp, D. M.; Bao, Z. *Chem. Mater.* **2008**, *20*, 2763–2772.

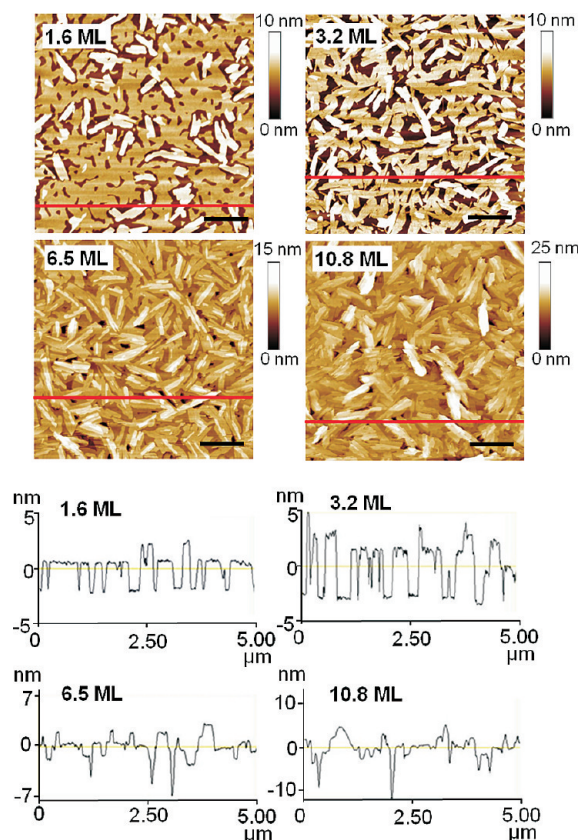


Figure 2. Tapping-mode AFM images of PDI-CN₂ thin films for various nominal thicknesses on OTS-treated SiO₂/Si substrates. The scale bar length is 1 μm. Note the larger z-axis scale (height) compared to Figure 1.

$\gamma = 90.3^\circ$. For all the thicker films, the entire multilayer observed in the AFM images forms the triclinic unit cell. A unit-cell angle γ slightly larger than 90° can be confirmed from the splitting of the (11L) and (1 $\bar{1}$ L) diffraction rods. The shape of the elongated Bragg diffraction spots (sharp along q_{xy} and slightly diffuse along q_z) arises from two effects. Both the small thickness of the film and the likely presence of stacking defects along the c-direction broaden the peaks along q_z .³⁶

The angular dependence carbon K-edge NEXAFS spectra were recorded at five different incident angles: 20 (grazing), 40, 55, 70, and 90° (normal). Labeled spectra of PDI films obtained at $\Theta = 13.7$ ML are shown in Figure S1 (see the Supporting Information). Since the PDI-F molecule has a PDI core that is substituted by two CH₂C₄F₉ end groups, the carbon K-edge NEXAFS spectra have rich features that originated from its C=C σ^* plane as well as C=C π^* vector orbitals of a PDI core, and C–C (or C–F) σ^* vector orbitals of the two end groups. The resonance peaks located in the region of 280–290 eV (region I) are mainly associated with the resonance orbitals of the PDI core, whereas those in the region of 290–305 eV (region II) are attributed to the resonance orbitals of the CH₂C₄F₉ end groups.³⁷ Table 1 summarizes the peak positions and their assignments. The spectra in region I contain six (main) peaks (for

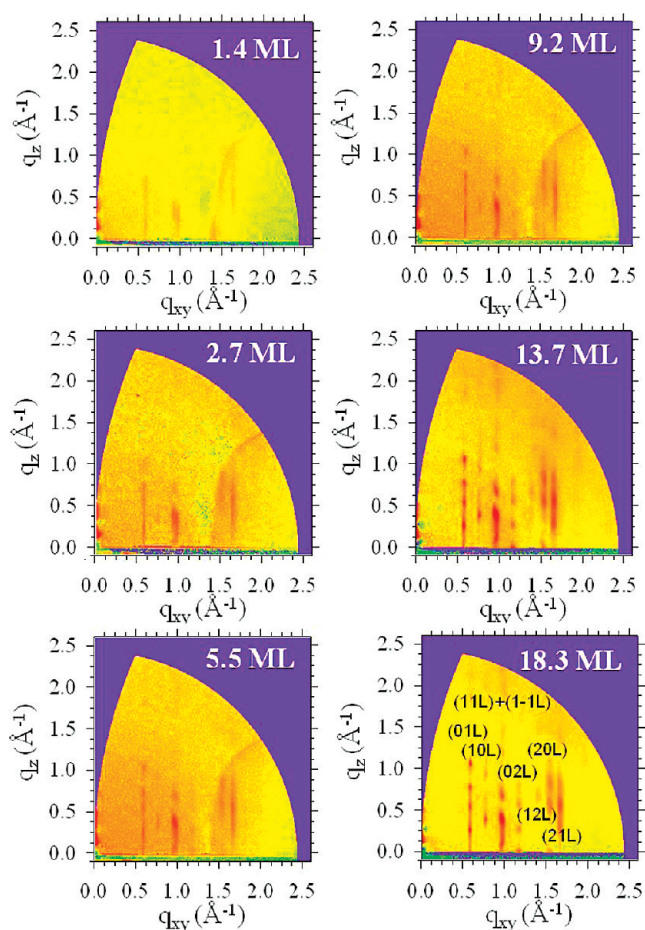


Figure 3. 2D GIXD patterns for PDI-F films of various thicknesses deposited on OTS-treated SiO₂/Si substrates.

briefly, the peaks are labeled as P-1, P-2, P-3, P-4, P-5, and P-6 in sequence). P-1 at 284.6 eV arises from transitions from the C1s levels to the LUMO (L_0) of the atoms labeled as a and c in Table 1, whereas P-2 at 284.9 eV arises from transitions from the atoms b and d into L_0 . P-3 at 285.8 eV corresponds to transitions from atoms e and f into L_1 and L_2 , whereas P-4 at 286.2 eV contains transitions from atoms c into L_3 and L_4 and also from atoms a and d into L_3 and L_4 . P-5 (287.8 eV) and P-6 (288.5 eV) are due to overlapped transitions from the anhydride/imide C atoms into L_0 and $L_1 + L_2 + L_3$, respectively.^{37–39} In region II, the sharp peak at 293.3 eV has been assigned to the C–F* absorption, and the peaks at 295.7, 297.8 eV are assigned to the C–C* and another C–F* absorption.⁴⁰

As the X-ray incidence angle moves from grazing to normal, the intensity of the π^* resonance peaks increases, indicating that the PDI core of PDI-F adopts vertical orientation on the surface. As a result, the horizontal orientation can be excluded. The nearly vertical orientations of PDI-F molecules were found regardless of the film thickness for our deposition conditions.

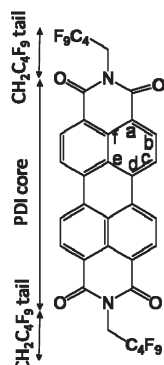
(37) Taborski, J.; Väterlein, P.; Dietz, H.; Zimmermann, U.; Umbach, E. *J. Electron Spectrosc. Relat. Phenom.* **1995**, *75*, 129–147.

(38) Zahn, D. R. T.; Gavrila, G. N.; Salvan, G. *Chem. Rev.* **2007**, *107*, 1161–1232.

(39) Scholz, M.; Schmidt, R.; Krause, S.; Schöll, A.; Reinert, F.; Würthner, F. *Appl. Phys. A: Mater. Sci. Process.* **2009**, *95*, 285–290.

(40) Gamble, L. J.; Ravel, B.; Fischer, D. A.; Castner, D. G. *Langmuir* **2002**, *18*, 2183–2189.

Table 1. Resonance Peak Assignments of PDI-F in the Carbon-K Edge NEXAFS Spectra^a

	Region	Peak no.	Photon Energy (eV)	Assignment
	PDI core (π^* -resonances)	1	284.6	a and c \rightarrow LUMO (L_0)
		2	284.9	b and d \rightarrow LUMO (L_0)
		3	285.8	e and f \rightarrow L_1 and L_2
		4	286.2	c \rightarrow L_1 and L_2 , and a and d \rightarrow L_3 and L_4
		5	287.8	imide C atoms \rightarrow L_0 and $L_1+L_2+L_3$
		6	288.5	imide C atoms \rightarrow L_5 and L_7
CH ₂ C ₄ F ₉ tails		7	293.3	σ^* (C-F)
		8	295.7	σ^* (C-C)
		9	297.8	σ^* (C-F')

^a The left drawing labels the positions of the different C atoms of PDI-F by letters a–f. In the PDI core assignment, transitions from the C1s levels of the atoms are labeled.

Because the GIXD data showed that PDI-F thin films on OTS-treated SiO₂/Si substrates had strong fiber texture (i.e., no crystallites with the *c*-axis in the plane of the substrate), a quantitative analysis of the grazing-angle dependence of the P-1 and P-2 peak intensities yields an azimuthally averaged molecular tilt angle of the PDI core of PDI-F. Following the process described in the literature,^{41,42} the molecular tilt angle (off the substrate normal) of the PDI core long axis for PDI-F thin films of various thicknesses can be calculated. These are approximately thickness independent and in a range of 16.7–24.8° (see Figure S2 in the Supporting Information). These data show that the long axis of PDI-F π -conjugated core adopts a nearly vertical orientation independent of film thickness, consistent with the GIXD.

It is more difficult to quantitatively analyze the tilt angle of the CH₂C₄F₉ from the NEXAFS spectra, because the C–C and C–F σ^* vector resonance peaks of the CH₂C₄F₉ group ends can overlap with those C=C analogue σ^* vector resonances of the PDI core in region-II. However, we believe the tilt angle (off the surface normal) of the end group should be larger than that of the PDI core for two reasons. The overall molecular length of PDI-F is computed as 2.56 nm, by MM2 energy minimization and PM3 geometry optimization. A layer spacing of 2.18 nm, derived from GIXD data, indicates a tilt angle of about 32° off surface normal, averaged over the molecule length. This angle is larger than that (21°) of the PDI core derived from the NEXAFS spectra. Since an average tilt angle of the entire PDI-F is \sim 32°, the tilt angles of the CH₂C₄F₉ end groups are most likely larger than 21°. However, the end chains must be tilted less than the “magic” angle of 54.7° away from surface normal;⁴¹ otherwise, the intensity enhancement of the C–C σ^* resonance (at 295.7 eV) with increasing incident angle would appear in the NEXAFS spectra. In fact, the angular dependence of the C–C σ^* peak intensity revealed an opposite trend to that of the C=C π^*

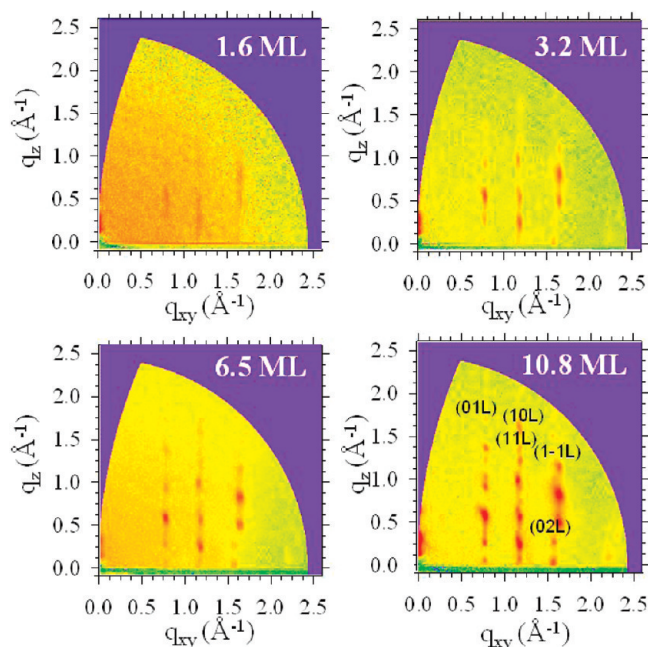


Figure 4. 2D GIXD patterns for PDI-CN₂ films of various thicknesses deposited on OTS-treated Si substrates.

resonances, indicating a preferential vertical orientation for both the PDI core and the CH₂C₄F₉ end groups. Nevertheless, in comparison with the C=C π^* resonances, the C–C σ^* resonance showed a weak angular dependence, supporting the argument that the end chains must be tilted more than the core off the surface normal.

GIXD and NEXAFS Analyses of PDI-CN₂. Figure 4 shows a series of 2D GIXD patterns for PDI-CN₂ films of various thicknesses on OTS-treated surfaces. All the patterns reveal rod-like scattering demonstrating typical strong fiber texture with cylindrical symmetry: the *c*-axis of the crystallites of PDI-F molecules is highly oriented with respect to surface normal. The GIXD pattern of the 1.6 ML film exhibiting three Bragg rods with positions at $q_{xy} = 0.82$ (01 L), 1.25 (10 L) and 1.71 Å^{−1} (1–1 L) indicates a typical 2D microstructure. As PDI-CN₂ grew into thicker films with thickness equal to 3.2 ML or

(41) DeLongchamp, D. M.; Lin, E. K.; Fischer, D. A. *Proce. SPIE* **2005**, 5940, 59400A.

(42) Stöhr, J.; Outka, D. A. *Phys. Rev. B* **1987**, 36, 7891.

Table 2. Resonance Peak Assignments of PDI-CN₂ in the Carbon-K Edge NEXAFS Spectra^a

region	peak no.	photon energy (eV)	assignment
PDI core (π^* -resonances)	1	283.9	a and c \rightarrow LUMO (L_0)
	2	284.6	b and d \rightarrow LUMO (L_0)
	3	284.9	e and f \rightarrow L_1 and L_2
	4	285.5	c \rightarrow L_1 and L_2 , and a and d \rightarrow L_3 and L_4
	5	287.1	imide C atoms \rightarrow L_0 and $L_1+L_2+L_3$
	6	287.9	imide C atoms \rightarrow L_5 and L_7
cyclohexane tails	7	292.5	σ^* (C–C)
	8	295.8	σ^* (C–C)
	9	303.9	σ^* (C–C)

^a In the PDI core assignment, the labels (letters a–f) of C atoms are same as in the case for PDI-F, and the transitions from the C1s levels of the atoms are assigned.

above, the GIXD patterns showed diffraction from sets of h , k , and l planes of a 3D crystal, which shows that the films form 3D crystallites with strong uniaxial (or fiber) preferred orientation about the substrate normal. The Bragg spots can be successively indexed based on a triclinic unit cell with dimensions: $a = 5.40$ Å, $b = 8.16$ Å, $c = 18.5$ Å, $\alpha = 94.5^\circ$, $\beta = 85.4^\circ$, and $\gamma = 110.6^\circ$. This is similar to that found for PDI-F films except that the a is half ($a = 10.3$ Å for PDI-F) reflecting a doubling of the in-plane unit cell for PDI-F. As observed in AFM images, the first layer of PDI-CN₂ has almost full coverage on OTS substrate, followed by the development of island terraces as thickness increases. The GIXD results are in good agreement with the AFM observations, because the films thicker than 3.2 ML reveal Bragg spots with sharp intensity profiles along both q_{xy} and q_z directions whereas the ultrathin film of 1.6 ML reveals several Bragg rods with diffuse intensity profiles along q_z .

NEXAFS spectra of a 10.8 ML-thick film of PDI-CN₂ grown on an OTS-treated SiO₂/Si substrate are shown in Figure S3. Since PDI-CN₂ molecule has one PDI core attached with two cyclohexyl end groups, the carbon K-edge NEXAFS spectra have features from its C=C σ^* plane as well as C=C π^* vector orbitals of a PDI core, and C–C σ^* vector orbitals of the cyclohexyl end groups. The carbon K-edge NEXAFS spectra for PDI-CN₂ can also be divided into two regions: region I (280–290 eV) and region II (290–320 eV). In region I, except for the two peaks at 286.6 and 286.9 eV, the other peaks attributed to C=C π^* vector orbitals exhibit higher intensities with increasing incidence angle.³⁷ In contrast, the two peaks at 286.6 and 286.9 eV show an opposite trend with increase in incidence angle. Region II mainly consists of C–C σ^* resonances of the cyclohexyl end groups at 292.5, 295.8, and 303.9 eV.⁴³ In region II, the σ^* features are most intense for grazing incidence light, but become the weakest in intensity for normal incidence, indicating a preferred vertical orientation of the cyclohexyl end groups. The summarized resonances are listed in Table 2.

Because each PDI-CN₂ molecule comprises a PDI core, dicyano and two cyclohexyl groups, the PDI-CN₂ spectra should contain a mixture of the resonances from the three functional groups. However, the features corresponding to C \equiv N π^* (287.85 eV) and σ^* (309.8 eV) resonances are less apparent in the carbon K-edge spectra.⁴⁴ This implies that the features for the C \equiv N fine structure are superimposed with those PDI and cyclohexane resonances. The superimposition of resonance adds difficulty in calculating tilt angles. Thus, only the first four peaks with positions at 283.9, 284.6, 284.9, and 285.5 eV were used to calculate the tilt angle of the PDI long axis. The angular dependence of the π^* peaks gives an average tilt value of $26^\circ \pm 3^\circ$ away from the surface normal. There is no clear dependence of tilt angle with deposition thickness (see Figure S4 in the Supporting Information).

OTFT Performance. Figure 5a exhibits field-effect mobility values of PDI-F TFTs in the saturation regime measured in N₂ atmosphere (solid squares) and air (open squares) as a function of the nominal film thickness. The average mobilities were obtained from at least three devices for each thickness. Below $\Theta = 1.8$ ML, no TFT behavior was observed in either N₂ or air atmosphere because of the absence of a percolation path for charge carriers in the channel, as shown by AFM images (Figures 1 and 2). In an N₂ atmosphere, a mobility of 2.75×10^{-4} cm² V⁻¹ s⁻¹ was observed at $\Theta = 2.3$ ML, and then increased rapidly with film thickness to ~ 0.07 cm² V⁻¹ s⁻¹ for films thicker than 3 ML. The blue solid line in Figure 5a represents a least-squares fit for μ measured under N₂ atmosphere to the empirical fitting equation given by Dinelli et al.²³

$$\mu = \mu_{\text{sat}} \left(1 - \exp \left[- \left(\frac{\Theta}{\Theta_0} \right)^\alpha \right] \right) \quad (2)$$

which yields a saturation thickness, $\Theta_0 = 2.9 \pm 0.4$ ML, a saturation value of the field-effect mobility, $\mu_{\text{sat}} = 0.071 \pm 0.002$ cm² V⁻¹ s⁻¹, and the exponent (a fitting parameter), $\alpha = 24.5 \pm 5.2$. In ambient air, PDI-F TFTs were not stable until the thickness increased up to ~ 10 ML. The red solid line in Figure 5a is a fit for μ values measured in air to eq 2, which gives a saturation thickness $\Theta_0 = 10.5 \pm 0.1$ ML, $\mu_{\text{sat}} = 0.061 \pm 0.001$ cm² V⁻¹ s⁻¹, and $\alpha = 7.2 \pm 0.4$. We used the power law ($\mu = a\Theta^\kappa + \epsilon$) to compare the relative increase of mobility before saturation in air-unstable region. The larger exponent, κ indicates the faster rise in μ . The dotted line is the power law fit to μ in air-unstable region with $\kappa = 2.4 \pm 0.4$.

Figure 5b plots μ for PDI-CN₂ TFTs measured in N₂ atmosphere (solid squares) and air (open squares, 1 h exposure) as a function of the nominal film thickness. The blue and red solid lines in Figure 5b correspond to the least-squares fit to eq 2 for μ measured in N₂ and air, respectively. In N₂, the empirical fitting analysis yields $\Theta_0 = 2.9 \pm 0.1$ ML, $\mu_{\text{sat}} = 0.86 \pm 0.02$ cm² V⁻¹ s⁻¹, and

(43) Hitchcock, A. P.; Newbury, D. C.; Ishii, I.; Stohr, J.; Horsley, J. A.; Redwing, R. D.; Johnson, A. L.; Sette, F. J. *Chem. Phys.* **1986**, *85*, 4849–4862.

(44) Stevens, P. A.; Madix, R. J.; Stohr, J. J. *Chem. Phys.* **1989**, *91*, 4338–4345.

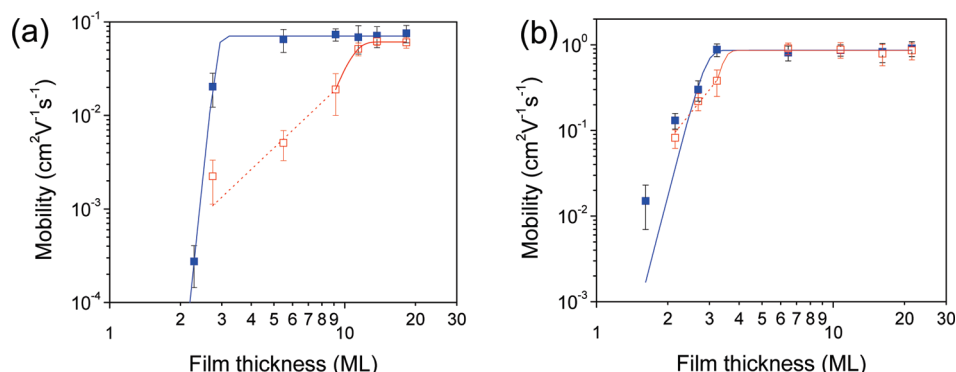


Figure 5. Field-effect mobility (μ) in an N₂ atmosphere (solid blue squares) and air (open red squares) as a function of the thickness of (a) PDI-F and (b) PDI-CN₂ films. The blue and red solid lines are fits to eq 2 for μ measured in N₂ and air, respectively, whereas the red dotted lines are power law fits in air-unstable region for μ in air. The measurements in air were performed in ambient lab environment (relative humidity $\sim 45\%$) at approximately 1 h after the removal from a glovebox filled with N₂ (O₂ level < 1 ppm).

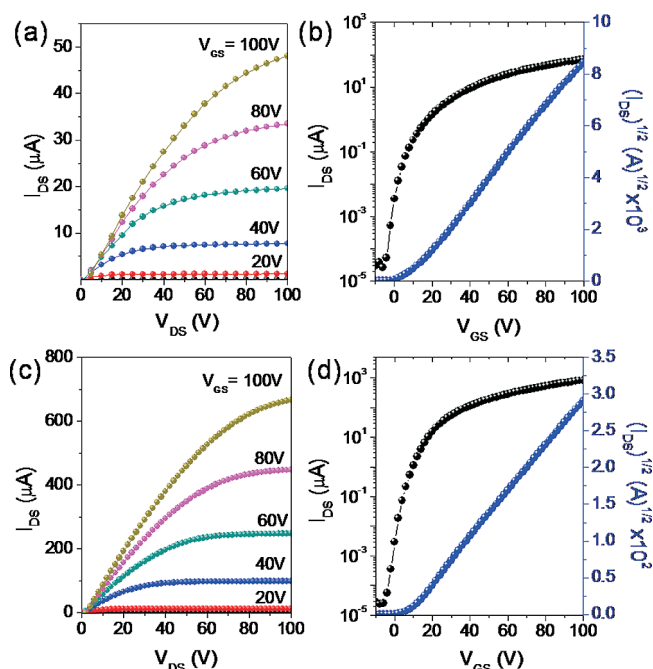


Figure 6. I – V characteristics of PDI-F and PDI-CN₂ TFTs. Output and transfer ($V_{\text{DS}} = 100$ V) characteristics for (a, b) PDI-F films (18.3 ML thickness) and (c, d) PDI-CN₂ films (6.5 ML thickness) were measured in an N₂ atmosphere.

$\alpha = 10.8 \pm 3.4$. In air, the empirical fitting leads to $\Theta_0 = 3.6 \pm 0.2$ ML, $\mu_{\text{sat}} = 0.86 \pm 0.02 \text{ cm}^2 \text{V}^{-1} \text{s}^{-1}$, and $\alpha = 4.3 \pm 1.0$. The dotted line is the power law fit to μ values in air-unstable region with $\kappa = 3.4 \pm 0.4$. At $\Theta = 1.6$ ML, PDI-CN₂ TFTs exhibited a mobility of $0.015 \text{ cm}^2 \text{V}^{-1} \text{s}^{-1}$ in an N₂ atmosphere, while those in air did not show any field-effect behavior. In addition, PDI-CN₂ TFTs prepared at $\Theta = 3.2$ ML showed a saturation mobility of $0.88 \text{ cm}^2 \text{V}^{-1} \text{s}^{-1}$ in N₂, whereas the mobility decreased by 57% in air when they were exposed to air for 1 h. However, PDI-CN₂ TFTs thicker than ~ 3.6 ML showed highly air-stable operation.

The output and transfer characteristics of PDI-F and PDI-CN₂ TFT devices with the highest mobilities obtained under N₂ atmosphere are illustrated in Figure 6. PDI-F TFTs exhibited a mobility as high as $0.092 \text{ cm}^2 \text{V}^{-1} \text{s}^{-1}$ with $I_{\text{on}}/I_{\text{off}}$ of 2.7×10^6 and V_{T} of 8 V, whereas PDI-CN₂ TFTs

showed the highest mobility of $1.03 \text{ cm}^2 \text{V}^{-1} \text{s}^{-1}$ with $I_{\text{on}}/I_{\text{off}}$ of 3.5×10^7 and V_{T} of 7 V. The mobility of PDI-CN₂ TFT is among the highest reported for air-stable n-channel OTFTs. Shukla et al. reported that cyclohexyl substituent in naphthalene diimide (NDI) increases the conformational rigidity of the overall molecule and assists in directing intermolecular stacking, leading to high field-effect mobility near $6 \text{ cm}^2 \text{V}^{-1} \text{s}^{-1}$.⁴⁵ However, cyclohexyl-NDI based TFTs were not stable in air, which was attributed to the energetically high-lying LUMO. Our saturated mobilities for PDI-CN₂ TFTs are higher than that obtained on 1,1,1,3,3,3-hexamethyldisilazane (HMDS)-treated SiO₂ dielectric ($0.1 \text{ cm}^2 \text{V}^{-1} \text{s}^{-1}$),¹¹ because our OTS surface modification layer is highly ordered and crystalline.³⁰ It is known that the phase⁴⁶ and the density⁴⁷ of the surface modification layer on the SiO₂ dielectric play an important role in controlling growth and crystallinity of organic semiconductors. In addition, as discussed earlier, the GIXD out-of-plane $d(100)$ -spacing (1.84 nm) is larger than that (1.79 nm) reported in the earlier.¹¹ This indicates the PDI-CN₂ molecules in the OTS-treated surface exhibit a smaller tilt angle relative to the substrate surface normal, which may be more efficient for charge transport.

Air Stability. The long-term air stabilities of PDI-F and PDI-CN₂ TFTs were monitored by measuring the performance as a function of time (Figure 7). PDI-F TFTs prepared with a nominal thickness of 2.3 ML only operated in N₂ atmosphere, whereas those prepared at 2.7 ML worked in air for several hours. After the nominal thickness of PDI-F films reached 5.5 ML, the TFTs functioned for about 1 month, despite the rapid performance degradation. PDI-F TFTs with nominal thicknesses larger than about 10 ML showed relatively long air-stable operation for about two months, but with similar performance degradation (an order of magnitude decay over the time period) regardless of the thickness.

(45) Shukla, D.; Nelson, S. F.; Freeman, D. C.; Rajeswaran, M.; Ahearn, W. G.; Meyer, D. M.; Carey, J. T. *Chem. Mater.* **2008**, *20*, 7486–7491.

(46) Lee, H. S.; Kim, D. H.; Cho, J. H.; Hwang, M.; Jang, Y.; Cho, K. *J. Am. Chem. Soc.* **2008**, *130*, 10556–10564.

(47) Virkar, A.; Mannsfeld, S.; Oh, J. H.; Toney, M. F.; Tan, Y. H.; Liu, G.-Y.; Scott, J. C.; Miller, R.; Bao, Z. *Adv. Funct. Mater.* **2009**, In Press.

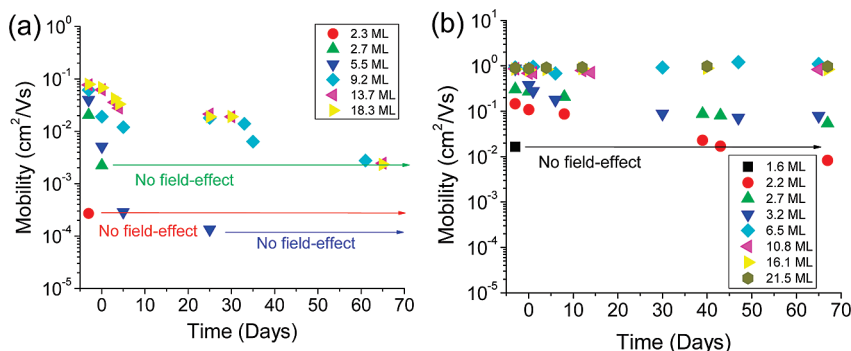


Figure 7. μ changes in air as functions of time for (a) PDI-F and (b) PDI-CN₂ TFTs prepared at various nominal thicknesses.

On the other hand, PDI-CN₂ TFTs exhibited two discrete regions for the air stability. Below about 4 ML, the air stability of PDI-CN₂ TFTs dropped remarkably with decreasing thickness and did not work in air at a nominal thickness of 1.6 ML despite of the presence of a percolation path, proven by the field-effect behavior obtained in an N₂ atmosphere. PDI-CN₂ TFTs with a nominal thickness of 3.2 ML degraded by 1 order of magnitude after exposing the devices to air for two months, which is similar to PDI-F TFTs with thicker layers ($\Theta \geq 10$ ML). However, PDI-CN₂ TFTs with a thickness over ~ 4 ML showed excellent air stability, with negligible mobility degradation.

Discussion

Although many mechanisms contribute to the air stability of n-channel OTFTs, two main factors are generally recognized: (i) the LUMO level, indicated by the first reduction potential, needs to be low to overcome ambient oxidation^{5,27,48–50} and (ii) the dense solid state packing, reduced number of grain boundaries, and shallow grain boundaries (i.e., do not penetrate all the way into the semiconductor/dielectric interface) are desirable for forming kinetic barriers to slow down and/or prevent the diffusion of ambient oxidants into the active channel area.^{11,15,51–55} For instance, Jones et al. reported that resistance to charge carrier trapping under ambient conditions for *N*-(n-octyl)arylene bisimide films occurs at a molecular reduction potential more positive than ~ -0.1 V versus SCE (LUMO ≤ -4.3 eV).⁵ They estimated that the overpotential for reaction of electron charge carriers with ambient oxygen in aryleneimide films is ~ 0.6 V, meaning that air-stable OTFT devices are potentially

achievable with arylene cores having the proper electron-withdrawing substituents. Anthopoulos et al. found that TFTs based on C₆₀ and C₇₀ derivatives showed air stability for molecules with LUMOs $\lesssim -4$ eV.⁴⁸ On the other hand, rylene dyes containing perfluorinated substituents in the imide position showed remarkable air stability for n-channel operation, although the fluorinated side chains do not significantly alter the LUMO energy levels ($\Delta E \leq 0.15$ eV).^{17,54} Katz et al. suggested that the larger van der Waals radius of fluorine atom relative to hydrogen atom results in a decreased available free spacing between the *N,N'*-chains from approximately 4 to 2 Å, thus hindering O₂ intrusion kinetically.¹⁵ More recently, Weitz et al. reported that these conventional interpretations are not sufficient to explain air stability in their PDI films.⁴ They found that the rate of mobility degradation in air was independent of the degree of molecular order in core-cyanated PDI films. This led them to propose that neither the redox potential nor the kinetic barrier is responsible for the air stability.⁴ The relatively low-lying LUMO levels of their core-cyanated PDI molecules are indeed within the empirical reduction potential windows required for air stability.^{5,27,48} In addition, there is a possibility that a dense, zigzag brick-type packing of their PDI molecules with the long axis arrangement parallel to the surface may also provide a kinetic barrier to the oxidants. Therefore, it is still unclear whether the same degradation rate is completely unrelated to the LUMO levels and the kinetic barriers. On the other hand, it is also uncertain how broadly the empirical chemical reduction potential window for air stability can be generalized to interpret the air stability of different types of n-channel organic semiconductors, since the reduction potentials for thin films are different from those measured in solution because of the electronic coupling between molecules in a solid state.²

In this study, to understand the thickness dependence of mobility and air stability of n-channel OTFTs, we used two n-channel organic semiconductors with distinct LUMO levels that correspond to different E_{R1} windows.^{5,27} The LUMO of PDI-CN₂ (-4.33 eV) falls within the air-stable region, whereas that of PDI-F (-3.84 eV) is at the onset region for air stability. Judging from Figure 5a, the field-effect mobility of PDI-F TFTs becomes saturated at about 3 ML under inert conditions. The V_T shift

- (48) Anthopoulos, T. D.; Anyfantis, G. C.; Papavassiliou, G. C.; Leeuw, D. M. d. *Appl. Phys. Lett.* **2007**, *90*, 122105.
- (49) Würthner, F. *Angew. Chem., Int. Ed.* **2001**, *40*, 1037–1039.
- (50) de Leeuw, D. M.; Simenon, M. M. J.; Brown, A. R.; Einerhand, R. E. F. *Synth. Met.* **1997**, *87*, 53–59.
- (51) Katz, H. E.; Bao, Z. N.; Gilat, S. L. *Acc. Chem. Res.* **2001**, *34*, 359–369.
- (52) Dimitrakopoulos, C. D.; Malenfant, P. R. L. *Adv. Mater.* **2002**, *14*, 99–117.
- (53) Oh, J. H.; Liu, S.; Bao, Z.; Schmidt, R.; Würthner, F. *Appl. Phys. Lett.* **2007**, *91*, 212107.
- (54) Katz, H. E.; Johnson, J.; Lovinger, A. J.; Li, W. *J. Am. Chem. Soc.* **2000**, *122*, 7787–7792.
- (55) Ling, M. M.; Erk, P.; Gomez, M.; Koenemann, M.; Locklin, J.; Bao, Z. N. *Adv. Mater.* **2007**, *19*, 1123–1127.

of PDI-F TFTs in air decreases with increasing the film thickness and converged to about +35 V after the thickness reaches ~ 10 ML (see Figure S5a in the Supporting Information). The degradation of PDI-F TFTs with time can be attributed to the intrusion of ambient oxidants such as O_2 , H_2O , and O_3 . It has also been demonstrated that organic films can exhibit a substantial morphological change after deposition on metals or SiO_2 .^{56–58} Although our AFM measurements did not reveal significant changes in the morphologies of PDI-F thin films aged over the stability-monitoring period, the crevice and the true depth between grains cannot be easily measured using AFM on thick films. Therefore, the post-deposition dewetting might also affect the temporal degradation. The gradual improvement in the air stability of PDI-F TFTs with increasing nominal film thickness reveals that the upper layers indeed serve as a kinetic barrier to the diffusion of environmental oxidants, even though they do not effectively contribute to the charge transport under an inert atmosphere.

The empirical fitting analysis of PDI-CN₂ TFTs reveals that the saturation of field-effect mobility is also accomplished at about 3 ML under inert conditions (Figure 5b). PDI-CN₂ is known as an air-stable n-channel semiconductor and its reduction potential is within the empirical window required for air stability.¹¹ However, TFTs based on the PDI-CN₂ ultrathin layer (≤ 4 ML) were still not stable in air, despite the existence of a percolation path as shown by the mobility in N_2 . The ultrathin layers less than 4 ML for the quasi-Stranski-Krastanov growth model are open to the intrusion of ambient oxidants. In addition, the surface molecules are more susceptible to reactions compared to molecules that are embedded in a crystal. It is well-known that many dye molecules fade rather rapidly with exposure by light while dye crystals (i. e., pigments) are much more stable. The major degradation path for dyes is photooxidation by oxygen. The V_T shift of PDI-CN₂ TFTs was also sensitive to the ambient exposure time for thicknesses below ~ 4 ML, and then converged to about +25 V at thickness over ~ 4 ML (see Figure S5b in the Supporting Information). This indicates that even for molecules with energetically low-lying LUMOs, we still need to consider the kinetic barrier for charge trapping by ambient oxidants. This becomes important at low film thickness. The V_T values of PDI-F and PDI-CN₂ TFTs both shifted to positive values over time, with relatively larger shift values in thinner layers because of the higher concentration of trapping species (see Figure S6 in the Supporting Information).

A schematic diagram for the three types of thin film growth modes is shown in Figure S7 of the Supporting Information. As shown by our AFM analysis discussed earlier, PDI-F film growth takes place in a quasi-layer-by-layer fashion (Frank-van der Merwe mode), whereas

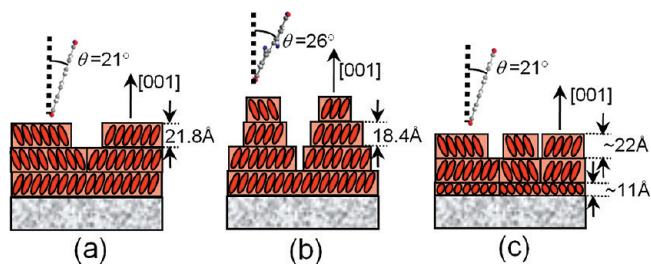


Figure 8. Schematic summary of the different thin film growth modes: (a) PDI-F on OTS-treated SiO_2 ; quasi-layer-by-layer (quasi-Frank-van der Merwe), (b) PDI-CN₂ on OTS-treated SiO_2 ; quasi-Stranski-Krastanov, and (c) PDI-F on bare SiO_2 ; the initial evolution is close to an island growth mode (quasi-Volmer–Weber), yet the overall growth is similar to quasi-layer-by-layer. θ is the average tilt angle of the PDI core with regard to the substrate normal.

PDI-CN₂ film growth follows quasi-Stranski-Krastanov mode on OTS-treated SiO_2/Si surfaces. Although the former is more desirable for the formation of kinetic barriers to the diffusion of ambient oxidants by providing more uniform high coverage, the latter showed better air stability. This indicates that electron affinity (LUMO level) becomes a dominant factor for the air stability above a critical thickness. To gain a better understanding of the effects of film growth and morphology on the air stability, we prepared PDI-F thin films on bare SiO_2/Si substrates without OTS treatment. AFM images of PDI-F film morphology on bare SiO_2/Si as a function of the nominal film thickness are shown in Figure S8. At $\Theta = 1.4$ ML, PDI-F on bare SiO_2/Si substrates exhibited smaller grains ($\sim 0.6 \mu m$ in the long axis) with a higher nucleating density compared to that on OTS-treated SiO_2/Si substrates ($\sim 1.3 \mu m$). Although the overall growth mode of PDI-F on bare SiO_2/Si was similar to the layer-by-layer mode, more nuclei for the second layer started to form at the initial growth ($\Theta < 2$ ML), displaying the initial evolution close to an island growth mode (Volmer–Weber). In addition, the step height of the first layer of PDI-F on bare SiO_2/Si was 1.1 ± 0.2 nm, while those of the following layers were 2.2 ± 0.3 nm. The PDI-F molecules in the first wetting layer are likely oriented with their long axis parallel to the substrate surface, so that the conjugated core of the molecule may not be protected efficiently by the fluoroalkyl chains from the ambient oxidants.⁴ In contrast, the molecules in the following layers are oriented with their long axis approximately upright on the substrate, similar to those on OTS-treated SiO_2/Si . Figure 8 illustrates the schematic summary of the PDI thin films grown on different conditions.

The mobility saturation ($0.035 \text{ cm}^2 \text{ V}^{-1} \text{ s}^{-1}$) of PDI-F TFTs on the bare SiO_2/Si was observed at an increased nominal thickness over ~ 6 ML (see Figure S9 in the Supporting Information). This is two times thicker than those on OTS-treated SiO_2/Si (~ 3 ML). The delay in formation of a percolation path and the maximum current may be related with unfavorable spatial correlations in the thin films due to the initial island growth.²³ The tilt angles of the long axis of the PDI π -conjugated core in the PDI-F films prepared on bare SiO_2/Si substrates were similar to those on OTS-treated substrate (Figure S10).

(56) Käfer, D.; Wöll, C.; Witte, G. *Appl. Phys. A: Mater. Sci. Process.* **2009**, *95*, 273–284.

(57) Käfer, D.; Ruppel, L.; Witte, G. *Phys. Rev. B* **2007**, *75*, 085309.

(58) Kowarik, S.; Gerlach, A.; Sellner, S.; Cavalcanti, L.; Schreiber, F. *Adv. Eng. Mater.* **2009**, *11*, 291–294.

However, the GIXD results showed more diffuse peaks along q_z , indicating the presence of stacking defects along the direction normal to the substrate. The field-effect mobility of PDI-F TFTs on the bare SiO_2/Si substrate degraded rapidly by more than 2 orders of magnitude after being stored in air for 2 months. The faster degradation of PDI-F TFTs on bare SiO_2/Si presumably originates from the facts that the PDI-F thin films on bare SiO_2/Si have smaller grains, a larger number of grain boundaries, and more defects in the solid-state packing, compared to those on the OTS-treated SiO_2/Si . In addition, the parallel orientation of the molecular long axis of the first layer molecules with regard to the substrate, in which the fluoroalkyl chains cannot act as an efficient barrier, may also be related with the faster degradation.

These observations suggest that it is important to consider multiple factors to understand the air stability of n-channel OTFTs including the LUMO level, molecular packing, film growth and morphology, and film thickness. Furthermore, molecular design and process strategy toward air-stable n-channel OTFTs should take into account all of these factors. We believe that our findings are not limited to the explanation of the air-stability mechanism for PDI semiconductors, but can be extended to those for other n-channel organic semiconductors.

Conclusions

We have investigated the effects of film thickness and morphology on the transistor performance and air stability for n-channel OTFTs using two PDI semiconductors (PDI-F and PDI-CN₂) that have distinctly different LUMO levels. AFM analysis revealed that PDI-F film growth takes place in a quasi-layer-by-layer fashion on OTS-treated SiO_2/Si substrates, whereas PDI-CN₂ film growth follows a quasi-Stranski-Krastanov mode. The average tilt angle (from the surface normal) of the long axis of PDI π -conjugated core for PDI-F and PDI-CN₂ thin films prepared on OTS-treated SiO_2 substrates were $\sim 21^\circ$ and 26° , respectively. PDI-F and PDI-CN₂ TFTs reached their saturated values of field-effect mobilities (0.071 and $0.86 \text{ cm}^2 \text{ V}^{-1} \text{ s}^{-1}$, respectively) at about 3 ML thickness under inert atmospheres. We found that the film thickness greatly affects the air stability of the TFT devices for both cases. The air stability of PDI-F TFTs, whose LUMO is at the onset of air-stable region,

increased drastically with increasing nominal thickness up to 10 ML, indicating that the thicker film acts as a kinetic barrier to the diffusion of ambient oxidants. The TFT performance of PDI-CN₂, having the LUMO well within the air-stable window and thus known as an air-stable n-channel organic semiconductor, was not stable in air if the active layer thickness was less than about 4 ML. PDI-F films on bare SiO_2/Si substrates exhibited smaller grains, larger number of grain boundaries, and more defects in the solid-state packing, leading to the faster degradation of the TFT devices compared to those on OTS-treated SiO_2/Si substrates. These observations show that the minimum thickness required for the air stability of n-channel organic semiconductors is closely related to the LUMO level of the active materials as well as the film growth mode and morphology. We found that n-channel semiconductors with an energetically low-lying LUMO level and/or a dense and larger crystal domain film can afford air-stable operation from thinner active layers. Our observations highlight the necessity of considering the interplay between multiple energetic and kinetic factors to understand the ambient stability of n-channel OTFTs.

Acknowledgment. Y.S.S. acknowledges financial support from the Taiwan Merit scholarship (NSC-095-SAF-I-564-626-TMS). Z.B. acknowledges financial support from BASF SE, the NSF-DMR solid state chemistry, and the Sloan Research Fellowship. F.W. acknowledges financial support from BASF SE and DFG. We also thank the Center for Polymeric Interfaces and Macromolecular Assemblies (NSF-Center MRSEC) for providing characterization facilities. Portions of this research were carried out at the Stanford Synchrotron Radiation Lightsource (SSRL), a national user facility operated by Stanford University on behalf of the U.S. Department of Energy, Office of Basic Energy Sciences.

Supporting Information Available: NEXAFS TEY spectral variations, average tilt angles of the long axis of π -conjugated core in PDI-F and PDI-CN₂ thin films prepared on OTS-treated SiO_2/Si , V_T variations of PDI-F and PDI-CN₂ TFTs as functions of film thickness, V_T changes as functions of time exposed to air, schematic diagram of three thin film growth modes, AFM topography of PDI-F thin films on bare SiO_2/Si , the tilt angles of the long axis of PDI π -conjugated core in PDI-F thin films deposited on bare SiO_2/Si , and thickness dependence of mobility of PDI-F TFTs prepared on bare SiO_2/Si (PDF). This material is available free of charge via the Internet at <http://pubs.acs.org>.